IOPscience iopscience.iop.org

Home Search Collections Journals About Contact us My IOPscience

Director distortion in a nematic wetting layer

This article has been downloaded from IOPscience. Please scroll down to see the full text article.

1996 J. Phys.: Condens. Matter 8 2741

(http://iopscience.iop.org/0953-8984/8/16/003)

View the table of contents for this issue, or go to the journal homepage for more

Download details:
IP Address: 171.66.16.208
The article was downloaded on 13/05/2010 at 16:32

Please note that terms and conditions apply.

J. Phys.: Condens. Matter **8** (1996) 2741–2754. Printed in the UK

Director distortion in a nematic wetting layer

F N Braun, T J Sluckin and E Velasco†

Faculty of Mathematical Studies, University of Southampton, Southampton SO17 1BJ, UK

Received 7 September 1995, in final form 5 December 1995

Abstract. Nematic liquid-crystal wetting at a solid interface presents particularly interesting features when the nematic director orientation at the solid interface is antagonistic to that favoured by the emerging nematic–isotropic interface. We have used the Landau–de Gennes theory of an inhomogeneous liquid crystal to make a quantitative study of this phenomenon, for the case when the solid surface favours homeotropic anchoring but the nematic–isotropic surface favours planar anchoring. By generalizing the theory of Sheng to allow spatial variation of the director, we find a richer surface phase diagram exhibiting a prewetting line or boundary transition shifted from that discussed by Sheng, as well as a transition between two nematic wetting phases, at which the wetting layer director profile changes from a homeotropic to a distorted texture.

1. Introduction

There has been an enormous amount of interest in recent years in wetting phenomena in fluids [1]. A particular case of this occurs in liquid-crystal-forming fluids just above the onset of nematic behaviour. In these fluids the surface may favour the nematic phase sufficiently to induce a nematic wetting layer which diverges as the temperature approaches the nematic–isotropic phase transition temperature T_{NI} [2, 3]. However, the liquid-crystal order parameter is a tensor, and this may affect the wetting characteristics.

One may imagine a case in which the nematic phase does indeed wet an interface, but where the director favoured by the wall is not the same as that favoured by the emergent nematic–isotropic interface. In this case the nature of the order parameter is a crucial determining factor of the wetting behaviour. Phenomenological studies of this problem by Sullivan and Lipowsky [4], and Sluckin and Poniewierski [5], using an interface Hamiltonian approach, indicate the possibility of a 'director-distorted' nematic liquid-crystal wetting phase. This phase is characterized by continuous rotation of the director between the two interfaces of an emergent nematic layer. This approach predicts that the thickness w of the nematic wetting layer behaves as $\Delta T^{-1/2}$ and the anomalous contribution to the surface tension γ as $\Delta T^{1/2}$, where $\Delta T = T - T_{NI}$ is the reduced temperature. In fact, as temperature is reduced there will be two wetting régimes. The high-temperature régime will be a thin nematic film whose width may not be diverging, or may diverge logarithmically with ΔT. As ΔT is reduced one expects a continuous phase transition to the director-distorted wetting phase.

For the case of strong homeotropic anchoring at a substrate (e.g. glass), logarithmic layer growth behaviour has been observed [6, 7]. This behaviour is in fact characteristic of scalar Landau-like theories of wetting. It can be contrasted with power-law layer growth

† Present address: Departamento de Física de la Materia Condensada, Universidad Autónoma de Madrid, E-28049 Madrid, Spain.

0953-8984/96/162741+14$19.50 © 1996 IOP Publishing Ltd

of the form $\Delta T^{-\beta}$, with $\beta < 0.5$, predicted to follow if van der Waals forces dominate [1]. One concludes therefore that in these experiments nearest-neighbour interactions between molecules dominate, and the director orientation is uniform [2, 3]. At a homeotropically anchoring substrate, a non-uniform director orientation in the wetting layer is driven by a tilted or planar texture at the free nematic–isotropic interface. This in turn is associated with particular values of the liquid-crystal elastic constants. Appropriate elastic constants of the liquid crystal might thus be expected to yield a crossover between the well-known logarithmic layer growth and the power law associated with director-distorted layers.

In this paper we make a closer analysis of the growth of these distorted wetting layers using the Landau–de Gennes formalism of inhomogeneous liquid crystals. This formalism has been used fruitfully in a number of recent papers to cast light on the systematics of wetting and anchoring phenomena involving nematic liquid crystals [8, 9, 10]. More specifically, in this paper, we shall use the model which has been closely analysed, albeit in a different context, by Sen and Sullivan [9]. We shall distinguish between: distorted nematic wetting layers (D); homeotropic layers which if extrapolated to T_{NI} would diverge in thickness, and which we thus denote as wetting homeotropic layers (H); and rather thin surface regions of enhanced homeotropic nematic order above T_{NI}, which are therefore partially wetting homeotropic layers (P).

The plan of this paper is as follows. In section 2 we describe the Landau–de Gennes model we use. In section 3 we briefly discuss the numerical method, and in section 4 the results of the calculations are presented. We show typical dependences of the nematic layer thickness and energy on temperature, and present relevant surface phase diagrams. Finally in section 5 we present some brief conclusions.

2. The Landau–de Gennes model

In this section we first recall the crucial features of the Landau–de Gennes formalism used by Sen and Sullivan [9]. We consider a semi-infinite system in which the substrate–liquid-crystal wall is located at $z = 0$, with the domain $z \geqslant 0$ corresponding to a nematic liquid crystal. There are two mathematically equivalent descriptions of the order parameter. We may use the components of the Saupe ordering matrix; this is equivalent to considering a laboratory-fixed frame of reference. Alternatively it may be more convenient to define a director angle, a principal order parameter and a degree of biaxiality; this is equivalent to considering a molecular frame of reference. The first is computationally simpler; the second is more intuitively helpful and is consistent with the macroscopic formulation of liquid-crystal theory.

We shall suppose the wall to be structureless and flat such that we may define an orthonormal triad $\boldsymbol{b}$, $\boldsymbol{c}$, $\boldsymbol{d}$, where $\boldsymbol{d}$ is the unit vector along $\boldsymbol{z}$ normal to the plane of the wall defined by $\boldsymbol{b}$ and $\boldsymbol{c}$. We shall suppose that no twist effects occur in the liquid crystal. In this case the vector $\boldsymbol{c}$ may be supposed to remain everywhere a principal axis of the nematic ordering tensor. There will now be three independent components to the ordering tensor. The ordering tensor can be described using three parameters $\eta(z)$, $\mu(z)$, $\nu(z)$ [11]. We may write

$$Q_{ij}(z) = \frac{\eta_s(z)}{2}(3d_i d_j - \delta_{ij}) + \frac{\sqrt{3}}{2}\mu_s(z)(b_i b_j - c_i c_j) + \frac{\sqrt{3}}{2}\nu_s(z)(b_i d_j + d_i b_j). \tag{1}$$

The alternative description involves the director angle $\psi(z)$. The tensor may be written

in terms of principal axes $\boldsymbol{n}(z)$, $\boldsymbol{l}(z)$ and $\boldsymbol{m}(z) = \boldsymbol{c}$:

$$Q_{ij}(z) = \frac{\eta(z)}{2}(3n_i n_j - \delta_{ij}) + \frac{\sqrt{3}}{2}\mu(z)(l_i l_j - m_i m_j) \tag{2}$$

with

$$\cos\psi = \boldsymbol{n} \cdot \boldsymbol{d}. \tag{3}$$

Transformation between the two frames can be achieved using the formula

$$\tan 2\psi(z) = \frac{2\nu_s(z)}{\sqrt{3}\eta_s(z) - \mu_s(z)}. \tag{4}$$

In Landau–de Gennes theory, the thermodynamics and equilibrium structure of the system are calculated by minimization with respect to the tensor $\boldsymbol{Q}(z)$ of a surface free-energy functional

$$F_s[\boldsymbol{Q}(z)] = \int_0^\infty \mathrm{d}z \ \left\{ f_l(\boldsymbol{Q}(z)) + f_{el}(\boldsymbol{Q}'(z)) + f_{sub}(\boldsymbol{Q}(z)) \right\} \tag{5}$$

where $\boldsymbol{Q}' = \mathrm{d}\boldsymbol{Q}/\mathrm{d}z$.

The first term is the Landau–de Gennes expansion of the bulk free-energy density [12]

$$f_l(Q) = A(T)Q_{ij}Q_{ij} - BQ_{ij}Q_{jk}Q_{ki} + CQ_{ij}Q_{ij}Q_{kl}Q_{kl} \tag{6}$$

where $A(T) = a(T - T^*)$ and the material constants a, B, C and T^* may be determined from experiment.

Contributions to the second term f_{el} are from elastic deformations across the ordered layer. In this study we focus on a form of the elastic energy which induces parallel orientation of the director at the nematic–isotropic (NI) interface of the wetting layer. The usual choice is that proposed by de Gennes [12], featuring two elastic constants L_1 and L_2:

$$f_{el}(\boldsymbol{Q}') = \frac{1}{2}L_1 Q'_{ij}Q'_{ij} + \frac{1}{2}L_2 Q'_{iz}Q'_{iz}. \tag{7}$$

For positive L_2, the free nematic–isotropic interface favours parallel director orientation, while negative L_2 favours homeotropic orientation. This form of the elastic contribution to the free energy does not permit an oblique tilt at the free nematic–isotropic interface, which can be imposed by including extra more complicated terms.

The final term in the functional is a substrate–liquid-crystal potential, for which we choose, in line with the model with a single scalar order parameter given by Sheng [3],

$$f_{sub}(\boldsymbol{Q}) = -g\delta(z)Q_{ij}d_i d_j. \tag{8}$$

For g positive, this may be interpreted as a short-range homeotropic anchoring potential. In general there are also surface terms quadratic in the order parameter [2], but we shall not need them in this study which concentrates on complete wetting by the nematic phase in a homeotropic texture.

In order to simplify the calculations and make contact with previous studies, it is convenient to use non-dimensional variables.

We define reduced temperature

$$t = 24A(T)C/B^2 \tag{9a}$$

with renormalized order parameters

$$\tilde{\eta}_s = 6C\eta_s/B \tag{9b}$$

$$\tilde{\mu}_s = 6C\mu_s/B \tag{9c}$$

and

$$\tilde{\nu_s} = 6C\nu_s/B \tag{9d}$$

and a new length scale

$$\tilde{z} = z/\xi \tag{9e}$$

with

$$\xi^2 = \frac{24C}{B^2}\left[L_1 + \frac{2}{3}L_2\right]. \tag{9f}$$

The free-energy density is now redefined by

$$\tilde{f_l} = \frac{B^4\xi^3}{576C^3} f_l \tag{9g}$$

and the surface anchoring parameter becomes

$$\tilde{g} = \frac{96C^2}{B^3\xi} g. \tag{9h}$$

We now drop the tildes, and obtain the following rescaled bulk free-energy density in the molecular frame of reference, equation (2):

$$f_\mathrm{l} = t(\eta^2 + \mu^2) - 2\eta(\eta^2 - 3\mu^2) + (\eta^2 + \mu^2)^2. \tag{10}$$

Biaxiality contributions to this are always positive, so biaxiality is suppressed in the limit of bulk homogeneity and we have

$$f_\mathrm{l} = \eta^2(\eta^2 - 2\eta + t). \tag{11}$$

The first-order bulk nematic–isotropic transition takes place at the reduced temperature $t_{NI} = 1$ with $\eta = 0$ and $\eta = 1$ defining the order parameter in the coexisting isotropic and nematic phases.

In the following calculations we consider only the effect of positive L_2 in competition with the homeotropic anchoring governed by positive g of equation (8).

The expression for f_el is now

$$f_\mathrm{el} = \frac{1}{2}\left(\frac{\mathrm{d}\eta_s}{\mathrm{d}z}\right)^2 + \frac{L}{2}\left(\frac{\mathrm{d}\mu_s}{\mathrm{d}z}\right)^2 + \frac{M}{2}\left(\frac{\mathrm{d}\nu_s}{\mathrm{d}z}\right)^2 \tag{12}$$

with the definitions

$$L = \frac{1}{1 + 2\kappa/3} \qquad M = \frac{1 + \kappa/2}{1 + 2\kappa/3} \tag{13}$$

where $\kappa = L_2/L_1$.

This rescaling causes the properties of a uniform homeotropic layer in which $\mu_s(z) = \nu_s(z) = 0$ to be invariant with respect to κ.

The substrate–LC interaction becomes

$$f_\mathrm{sub} = -g\eta_s(0). \tag{14}$$

3. Numerical method

We have minimized the free energy, equation (6), in the region just above the nematic–isotropic transition at $t = 1$, for various different values of the surface coupling g and the elasticity ratio κ. In general the order parameter profile consists of a region of thickness w close to the interface with an enhanced order parameter ~ 1 ('the nematic wetting layer'), a region of rapidly changing order parameter at a distance w from the interface ('the nematic–isotropic interface'), and a region with a very low order parameter ('the isotropic region') further still from the interface. For low coupling constants g and well above $t_{NI} = 1$ the first two features may be absent. When there is a wetting layer, it may be homeotropic or it may show director distortion.

In finding numerical solutions to the director-distorted case, the D phase, it turns out to be convenient to divide the minimization procedure into two levels.

On one level, the order parameter profile is discretized into a mesh of $3N$ variables with respect to which the minimization is carried out, i.e. $\eta_s^i = \eta_s(z^i)$, $\mu_s^i = \mu_s(z^i)$, $\nu_s^i = \nu_s(z^i)$; $i = 1, \ldots, N$; $z_i = hi$ etc.

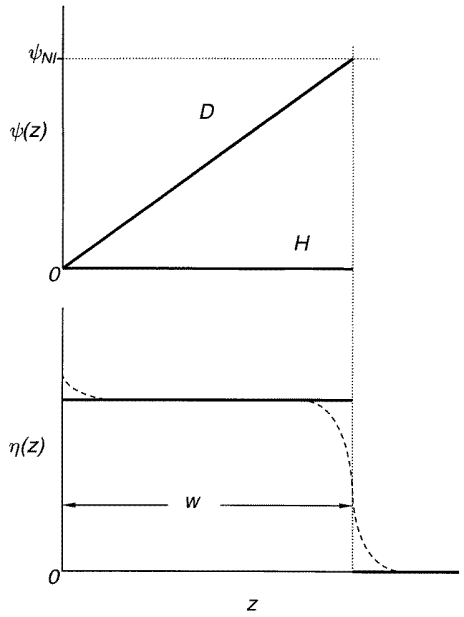

Figure 1. A schematic diagram of the initial profile, showing 'slow' variables w and Ψ_{NI}. The order profile is initially a step function, shown as the solid line in the lower part of the diagram. Smoothing yields equilibrium structure (the dashed line). The upper part of the diagram shows the corresponding director profiles associated with D solutions.

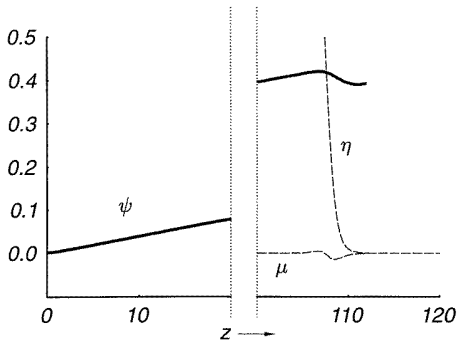

Figure 2. Equilibrium structure at the interfaces after full minimization with respect to the order parameter profile; $\kappa = 2$, $g = 0.2$, $t = 1.0002$.

A conjugate gradient method [13] was used to minimize these $3N$ variables for given layer thickness w, and angle of tilt at the nematic–isotropic interface Ψ_{NI}. These latter two quantities are 'slow variables'; the energy is very weakly dependent on them. Compounded by the assumption that the director tilt $\psi(z)$ varies more or less linearly with distance from the interface, the two slow variables describe an initial profile from which the $3N$-

dimensional conjugate gradient minimization starts. The $3N$-dimensional minimization, however, primarily acts to smooth variables which are discontinuous in the initial profile. The main effect is to alter the details of the order parameter profile at the incipient nematic–isotropic interface and close to the wall. We therefore nest this smoothing procedure inside a higher-level minimization with respect to w and ψ_{NI}.

In figure 1, the solid lines show the initial-profile schematic diagram governed by w and ψ_{NI}. We have used the same approach to calculate homeotropic (H) solutions (using only a single slow variable w, of course).

The assumption of constant $\mathrm{d}\psi/\mathrm{d}z$ is seen to be a good approximation by expanding equation (7) in the molecular frame of reference, i.e. with respect to ψ and η. In the bulk of the layer, where $\mathrm{d}\eta/\mathrm{d}z \approx 0$, the leading-order contribution to the elastic free-energy density is in $(\mathrm{d}\psi/\mathrm{d}z)^2$:

$$f_{\mathrm{el}} \approx \frac{9(2+\kappa)}{4(3+2\kappa)} \left(\frac{\mathrm{d}\psi}{\mathrm{d}z}\right)^2 . \tag{15}$$

When integrated over the layer width, this contribution is minimized by the condition $\mathrm{d}\psi/\mathrm{d}z = \text{constant}$.

The smoothing process described yields relaxed $\eta(z)$-structure at the respective interfaces, which we show schematically in figure 1 by the dashed line. There is also relaxation in $\psi(z)$, but again the main effects are at the interfaces. This means that in practice we need only smooth over the interfacial regions, rather than over the complete set of $3N$ variables describing the system.

Figure 2 shows an example of the structure of the order parameter profile structure at the two interfaces of a fully minimized D solution. The director profile at both interfaces has relaxed away from the condition $\mathrm{d}\psi/\mathrm{d}z = \text{constant}$ implemented in the initial-profile schematic diagram (figure 1). This relaxation is considerably weaker at the NI interface than at the substrate. Biaxial structure is in evidence at the NI interface, but not at the substrate. There is enhanced uniaxial order at the substrate, but this is not shown.

An important point concerns the condition $\psi(0) = 0$ which we have prescribed in the initial profile. The homeotropic texture is favoured from the condition $g > 0$. However, the onset of director distortion is expected to destroy this symmetry. While one certainly expects $\psi(0)$ to be non-zero after proper minimization, the question arises as to whether the homeotropic anchoring is sufficiently strong that $\psi(0)$ is *negligible* and the numerical method that we have outlined remains well founded. This is important because although the numerical method can be relied upon to relax by small amounts, it cannot converge to a solution which is significantly removed from the initial profile.

An instructive way to address the issue is to consider the anchoring energies W_s^{sub} and W_s^{NI} associated with the respective interfaces. If $W_s^{NI}/W_s^{\mathrm{sub}} \ll 1$, then the stronger anchoring at the substrate dominates and $\psi(0) \sim 0$. Within the model, we have more or less independent control of these anchoring strengths via the parameters g and κ. By increasing κ we increase W_s^{NI}, whereas by increasing g we increase W_s^{sub}. Thus the above ratio is maximized in the limit $g \to 0$ and $\kappa \to \infty$.

With these considerations in mind, we have roughly estimated the range of validity of the assumption $\psi \sim 0$ by performing calculations which implement $\psi_0 \sim \psi(0)$ as a third slow variable. This is shown in figure 3(a). For fixed $\kappa = 20$, $g = 0.2$, the director tilt at the respective interfaces is plotted against width w. The width in this plot is controlled by varying temperature. As one expects intuitively, as w increases and the interfaces move apart, both tilts relax towards their preferred orientations. A rough estimate of the lower limit above which we can reasonably assume $\psi(0) \sim 0$ might be, for this example, $w \approx 30\xi$.

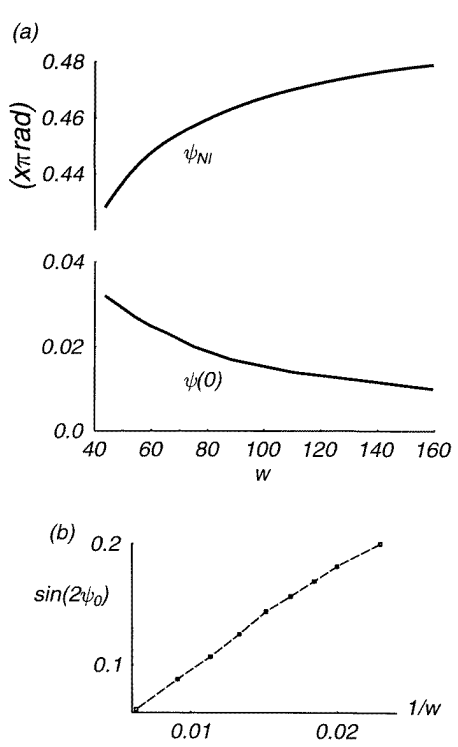

Figure 3. (a) The width dependence of the director tilts at the substrate ($\psi(0)$) and the NI interface (ψ_{NI}); $\kappa = 20$, $g = 0.2$. (b) The same data replotted to demonstrate the near-linear behaviour $\sin(2\psi(0)) \sim 1/w$.

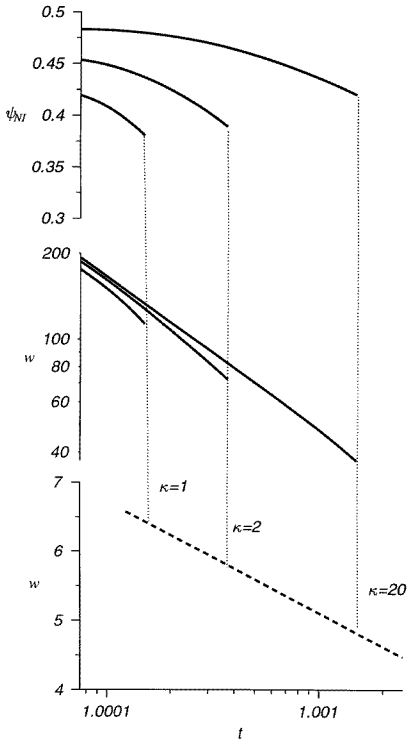

Figure 4. Representative plots showing the first-order jumps (dotted lines) in layer thickness as the director profile reconfigures. The director-distorted profiles (solid lines) are stable at lower temperatures, exhibiting the -0.5 scaling exponent in the limit $t \to 1$. The homeotropic layer (dashed line) exhibits logarithmic behaviour. The width scale may alternatively be viewed as a negative surface entropy scale. $g = 1.5$ (i.e. pertaining to complete wetting).

In the results presented in the next section, we find that the D phase is no longer stable at this width. In fact this choice of g and κ reflects as high a ratio $W_s^{NI}/W_s^{\text{sub}}$ as one can hope to achieve without straying beyond the extremes of D-phase stability (regardless of width and temperature). This allows us to assume $\psi(0) \sim 0$ over the entire parameter space. From a numerical perspective we conclude that there is no need for a third slow variable ψ_0.

A useful check on our numerical approach in general can be achieved from a comparison with the analytical result which follows from assuming uniform $\eta(z) = 1$ over the layer width $0 < z < w$. Equation (14) may then be written as

$$f_{\text{sub}} = -g P_2(\cos\psi(0)) \tag{16}$$

where P_2 denotes the second Legendre polynomial.

Substituting this, along with equation (15), into the functional given as equation (5), we obtain by variational minimization the Euler–Lagrange condition at the substrate surface:

$$\frac{\mathrm{d}f_{\text{sub}}}{\mathrm{d}\psi(0)} = \frac{9(2+\kappa)}{2(3+2\kappa)}\frac{\mathrm{d}\psi}{\mathrm{d}z}. \tag{17}$$

For large κ, this leads to the relation

$$\sin(2\psi(0)) \approx \frac{3}{2g}(\psi_{NI} - \psi(0))\frac{1}{w}. \tag{18}$$

Figure 3(b) shows $\sin(2\psi_0)$ versus $1/w$ for the data of figure 3(a), i.e. $g = 0.2$, $\kappa = 20$. Substitution of $g = 0.2$ and $\psi_{NI} - \psi(0) \approx \pi/2$ into equation (18) gives $\sin(2\psi_0) \approx 10/w$. This is consistent with the gradient of the graph. The figure also exhibits a slow decrease in the gradient reflecting the decrease in $\psi_{NI} - \psi_0$.

4. Results

We recall the different types of solution for $\boldsymbol{Q}(z) = [\eta(z), \mu(z), \nu(z)]$. In the P and H surface phases the director is uniformly homeotropically oriented throughout the layer. In the D surface phase $\psi(0) \sim 0$ at the substrate, with $\psi(z)$ roughly monotonically increasing at constant gradient $\mathrm{d}\psi/\mathrm{d}z =$ constant up to an angle ψ_{NI} at the NI interface.

In figure 4 we show plots of the thickness $w(t)$, for a fixed value of $g = 1.5$ and for three different values of κ. This value of g is sufficiently large that the homeotropic layer thickness diverges; the nematic phase wets the wall. In order to present the results in the most effective way, the temperature scale is plotted on a logarithmic scale in $(t - 1)$. The dashed line that is the lowest curve represents the growth of a homeotropic layer. In the lowest of the three graphs the layer thickness scale is presented linearly. This dashed curve is linear, indicating that $w \sim \ln(t - 1)$. The homeotropic layer (which from the scaling is invariant with respect to change in κ), is diverging at $t = 1$.

Thus, well above the nematic–isotropic phase transition, the H phase is stable. However, as the temperature is reduced, the new D phase replaces it. This occurs at higher temperatures if κ is increased. This is shown in the middle graph in figure 4. In this graph the thickness w is also presented on a logarithmic scale. These graphs now also show a linear behaviour as $t \to 1$, with a gradient of -0.5. This indicates that $w \sim (t - 1)^{-1/2}$, diverging with a power law as predicted [4, 5].

However, the transition between the two phases is not continuous, but rather has a strong first-order character. For example, for $\kappa = 2$ the transition occurs at $t = 1.000\,36$ between $w \sim 6\xi$ in the H phase to $w \sim 74\xi$ in the D phase. We have also plotted the tilt angle at the nematic–isotropic interface ψ_{NI}, in the distorted layer. As the coexistence limit $t = 1$ is approached the layer thickness w becomes very thick, the nematic–isotropic interface and the nematic–wall interfaces are far apart, and ψ_{NI} relaxes towards $\pi/2$. We see that this tilt does decrease slightly with temperature down to $\psi_{NI} \approx 0.39$ at the HD transition, indicating a balance between the anchoring energy at the nematic–isotropic interface and the elastic energy in the distorted wetting layer. However, it never reduces to zero, as it would in a continuous transition.

We show in figure 5 the surface free energy F_s associated with one of the nematic layers ($\kappa = 2$) shown in figure 4. This quantity plunges dramatically in the neighbourhood of t_{NI}, as the nascent nematic–isotropic interface in the thickening wetting layer is now increasingly able to exhibit its preferred orientation. As we show in this figure, the degree of reduction of F_s is almost exactly the difference between the nematic–isotropic surface free energies at homeotropic and planar anchoring—the anchoring energy at the nematic–isotropic interface. This is not surprising; in the limit $t \to 1$ the major change in the contribution to the surface free energy comes from the nematic–isotropic surface at the edge of the nematic wetting layer. We also observe that the gradient $\mathrm{d}F_s/\mathrm{d}t$ diverges as $t = 1$ is approached. This

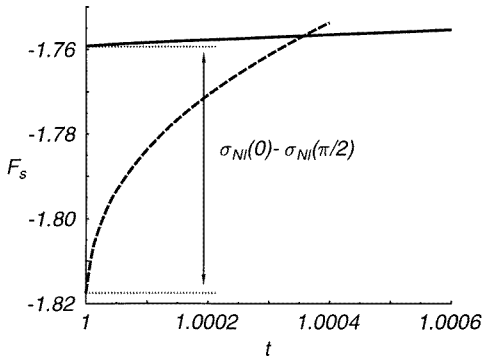

Figure 5. The surface free energy in the complete wetting régime as t_{NI} is approached, showing the first-order H–D (solid line–dashed line) transition; $\kappa = 2$, $g = 1.5$.

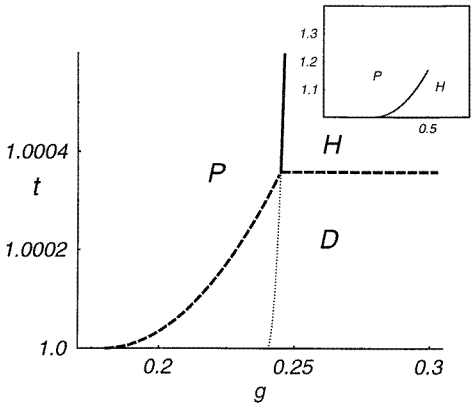

Figure 6. The prewetting phase diagram showing the modification of the Sheng prewetting line by the effects of director distortion. The unmodified prewetting line is shown in the inset for comparison. With respect to the surface critical point, the D surface phase is stable only at temperatures very close to t_{NI}. Hence the main diagram is plotted on a significantly smaller scale. The dotted line depicts the part of the prewetting line which disappears to be replaced by a PD prewetting line (curved dashed line). Both the old and the new prewetting lines have zero gradient in the limit of t_{NI}. A surface triple point features in the modified diagram, off which extends a horizontal line of HD layer transitions. $\kappa = 2$.

divergence also goes as $(t-1)^{-1/2}$; phenomenological analyses of wetting layers [4, 5] predict that $\mathrm{d}F_s/\mathrm{d}t$ and w should diverge with the same power law.

We can draw together the general picture of the behaviour of wetting films as a function of temperature t and surface ordering parameter g by plotting a wetting phase diagram, showing the regions in which the P, H, and D surface phases are stable. A useful reference point on which to base our discussion is the wetting phase diagram described by Sheng [3, 14]. This model restricts discussion to P and H surface phases. The nematic wetting transition, at which the H phase pre-empts the P phase at nematic–isotropic coexistence, occurs at $g = g_H^W \approx 0.24$. The prewetting line, which Sheng called the boundary phase transition, is a first-order surface phase transition separating the P and H regions. It extends from the wetting transition at $g = g_H^W$, $t = t_{NI}$ to a surface critical

point at $g = 0.5$, $t = 1.17$.

However, for $\kappa > 0$ a D surface phase is in principle permitted. We show in figure 6 the resulting altered surface phase diagram for $\kappa = 2$, with the features of the original Sheng wetting phase diagram also marked. The principal new features of the modified phase diagram are: (a) for all values of g in which the H phase wets the interface in the original Sheng picture, the H phase is pre-empted by a wetting D phase at $t = t_{HD} \approx 1.000\,36$; (b) because the nematic–isotropic surface tension is lower for a planar orientation, the wetting transition occurs at a lower value of $g = g_D^W \approx 0.18$; (c) there is a modified prewetting line extending from the modified wetting transition which divides the partial wetting P films from the wetting D layer, along a line $t = t_{PD}(g)$; (d) this modified prewetting line meets the original Sheng prewetting line and the HD line at a surface triple point at $g = g_{tr} \approx 0.24$, $t = t_{tr} = t_{HD} \approx 1.000\,36$; (e) above t_{tr} the Sheng prewetting line continues up to the original surface critical point.

The modified surface phase diagram is thus seen to be considerably richer than the original Sheng surface phase diagram. In what follows we discuss some of the features of this phase diagram in more detail.

4.1. Features of the modified surface phase diagram

Two noteworthy features of figure 6 are: (a) t_{HD} is extremely insensitive to g over the complete wetting region of the surface phase diagram; and (b) by contrast, in the partial wetting regime, $t_{PD}(g)$ exhibits a rather weaker dependence on g than the original Sheng prewetting line $t_{PH}(g)$. In what follows we carry out a more careful analysis of the expected dependence of these surface phase boundaries.

This analysis can be carried out by developing a Clausius–Clapeyron-type equation governing the surface phase boundaries. The condition for coexistence $\mathrm{d}F_s^A = \mathrm{d}F_s^B$ between two surface phases A and B in the t–g plane, combined with equation (8), yields

$$\frac{\mathrm{d}t}{\mathrm{d}g} = \frac{\partial F_s^B/\partial g - \partial F_s^A/\partial g}{\partial F_s^A/\partial t - \partial F_s^B/\partial t} = \frac{\eta^A(0) - \eta^B(0)}{S_s^B - S_s^A} = -\frac{\Delta\eta}{\Delta S_s} \tag{19}$$

where $\eta^A(0), \eta^B(0)$ are the order parameters at $z = 0$, S_s^A, S_s^B are the respective surface excess entropies corresponding in the model to

$$S_s = -\frac{\partial F_s}{\partial t} = -\int_0^\infty \mathrm{d}z\ \{Q_{ij}(z)Q_{ij}(z)\} = -\int_0^\infty \mathrm{d}z\ \{\eta_s^2(z) + \mu_s^2(z) + \nu_s^2(z)\} \tag{20}$$

and $\Delta\eta$ indicates changes in quantities across the surface phase boundary.

For wetting layers, the quantity S_s is approximately:

$$S_s \approx -\int_0^\infty \eta^2(z)\ \mathrm{d}z \approx -w. \tag{21}$$

Thus the magnitude of the surface entropy S_s is approximately the thickness of the nematic layer at the interface.

We can now use the result of equation (21) to elucidate the features of figure 6. We first discuss the flatness of the line t_{HD}. In this case both the H and D phases are wetting phases, and $\eta(0) \approx 1$ in both cases; we expect that $\Delta\eta < 0.1$. However, the transition is between phases with very different values of w; we have found numerically that $\Delta w \sim 70$ for realistic values of κ. We thus find that

$$\frac{\mathrm{d}t}{\mathrm{d}g} = \frac{\Delta\eta}{\Delta w} \sim 1.4 \times 10^{-3} \ll 1. \tag{22}$$

We now examine $t_{PD}(g)$. In the partial wetting regime, by contrast to the wetting régime, we have $\eta(0) \sim 0$, and $w \sim 1$. Thus, now

$$\frac{\mathrm{d}t}{\mathrm{d}g} \sim \frac{1}{w_D}. \tag{23}$$

At the surface triple point $w_D \sim 70$, and we see that the dependence on g is very much stronger than at the distortion transition from the H wetting phase. However, as the wetting transition point is approached w diverges, leading to the expected relation $t_{PD} \sim (g - g_D^W)^2$, with zero gradient as the wetting transition is approached.

We can also estimate the shift $\Delta g^W = g_H^W - g_D^W$ of the wetting transition following from considering the possibility of the D surface phase. The wetting transition occurs as a result of balancing the increase in surface free energy resulting from adding a nematic–isotropic interface with the decrease as a result of having a high surface order parameter.

If we roughly suppose that these are the only two contributions, and that $\eta(0) \sim 1$ in the wetting phases and $\eta(0) \sim 0$ in the non-wetting phases, we obtain for the surface free energy along $t = 1$

$$F_s(P) \approx 0 \tag{24a}$$

$$F_s(H) \approx \sigma_{NI}(0) - g \tag{24b}$$

$$F_s(D) \approx \sigma_{NI}(\pi/2) - g \tag{24c}$$

where $\sigma_{NI}(\theta)$ denotes the surface free energy at the nematic–isotropic interface with the surface tilt angle at angle θ.

Comparing these equations we obtain

$$\Delta g^W \sim \sigma_{NI}(0) - \sigma_{NI}(\pi/2) = W_s^{NI} \tag{25}$$

where W_s^{NI} is the anchoring energy at the nematic–isotropic interface.

The shift Δg^W is κ-dependent via $W_s^{NI} \sim \kappa$. In the next section we examine the role of κ more quantitatively.

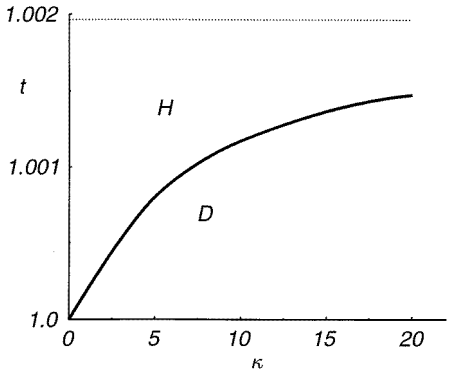

Figure 7. A projection of the prewetting phase diagram in the κ–t plane, with the surface field g fixed in the complete wetting regime. Both H and D are complete wetting phases, but H wetting is superseded by D wetting for all positive κ. The physically relevant range of κ is thought to be 2–4, where the coexistence line is approximately linear. In the high-κ limit, the coexistence temperature t_{HD} tends towards a maximum just below $t = 1.002$ (dotted line).

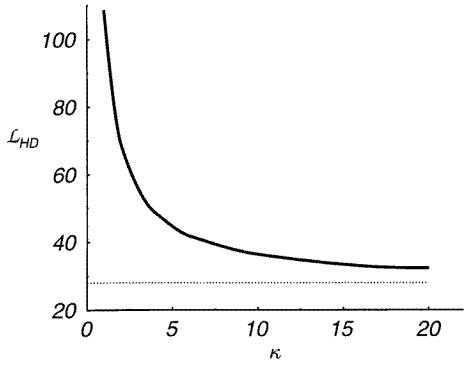

Figure 8. Latent heat along the coexistence line of the previous figure. Again, an asymptotic limit exists at high κ (dotted line). In the low-κ limit, the latent heat diverges.

4.2. The elastic constant–temperature plane

In figure 7 we show the projection of the wetting phase diagram in the κ–t plane. As long as the surface field g is sufficiently high to ensure complete wetting by the nematic phase, this is insensitive to g. For all positive κ, we see that complete wetting by H is superseded by complete wetting by D.

The HD surface phase boundary tends to an asymptotic limit $t \approx 1.002$ as $\kappa \to \infty$, shown by the dotted line. The fact that such an asymptotic limit exists may be explained in the following way. The quantities L and M defined in equation (13) approach constant values of 1 and 3/4 respectively in the limit $\kappa \to \infty$. Then, using equation (12), the system becomes independent of κ:

$$\lim_{\kappa\to\infty} f_{\mathrm{el}} = \frac{1}{2}\left(\frac{\mathrm{d}\eta_s}{\mathrm{d}z}\right)^2 + \frac{3}{8}\left(\frac{\mathrm{d}\nu_s}{\mathrm{d}z}\right)^2. \tag{26}$$

This upper bound on the HD surface phase transition temperature is well below the surface critical point at which the Sheng prewetting line (PH) terminates. Our model therefore exhibits the PHD triple point for all $\kappa > 0$.

We have also plotted, in figure 8, the latent heat $\mathcal{L}_{HD}$ along the HD surface phase boundary. Again, as $\kappa \to \infty$, the asymptotic limit of f_{el} imposes a lower bound on the latent heat of $\approx$28 (dimensionless units). The quantity $\mathcal{L}_{HD}$ diverges as $\kappa \to 0$.

Let us briefly review the reason for the divergence of $\mathcal{L}_{HD}$. From equation (21), the latent heat may be regarded as essentially the jump Δw in nematic layer width at the phase transition. This jump exhibits the 0.5 power-law divergence in the $t = 1$ limit, because the D layer power-law behaviour dominates the logarithmic divergence of the H layer. The HD transition occurs as a balance of nematic–isotropic interface anchoring energy W_s^{NI}, which favours the D surface phase, against director curvature energy, which favours the H phase. The HD transition will thus occur when $W_s^{NI} \sim w_D^{-1}$. Hence

$$\mathcal{L}_{HD} \sim w_D \sim (W_s^{NI})^{-1} \sim \kappa^{-1}. \tag{27}$$

4.3. An order-of-magnitude estimate

It remains to convert our findings into an estimate of real liquid-crystal properties. We substitute the following values obtained experimentally for MBBA [16] for the Landau–de

Gennes coefficients appearing in equation (6): $a = 0.030$ J cm^{-3}, $B = -0.263$ J cm^{-3}, $C = 0.136$ J cm^{-3} and $T^* = 318.3$ K. The physically relevant range of κ is thought to be 2–4 [9], over which the coexistence line of figure 7 is approximately linear. Thus, we obtain for the HD transition temperature

$$T_{HD} \approx T_{NI} + \frac{B^2\kappa}{24aC}\frac{\mathrm{d}t_{HD}}{\mathrm{d}\kappa} \approx (318.3 + 1.6\kappa \times 10^{-4})\ \mathrm{K}. \tag{28}$$

We note, however, that MBBA is not an entirely appropriate choice since *oblique* anchoring at the free nematic isotropic interface has been observed [15] in addition to the planar anchoring that we require for consistency with the present theory. Nevertheless, this serves as an order-of-magnitude estimate of the size of the phenomenon.

5. Conclusion

We have solved a Landau–de Gennes theory model for a liquid-crystal-forming material close to an interface, for temperatures just above t_{NI}. We have concentrated on a régime for which the surface favours homeotropic anchoring, but the nematic–isotropic boundary favours planar anchoring. We then examined, in particular, solutions for which there is a nematic layer close to the interface which diverges as the clearing point is approached.

Our primary concern has been to test, in a more systematic way, predictions made using an interface Hamiltonian approach. These calculations indicated that a growing homeotropic layer would be superseded, very close to t_{NI}, by a distorted layer which is homeotropic at the surface, but planar or nearly so at the edge of the wetting nematic film. The two layers would have different divergence characteristics close to the bulk transition.

We have indeed found two types of solution corresponding to two qualitatively contrasting forms of the director profile, which correspond closely to the expected order parameter profiles, and which have the predicted power-law behaviour. We also find a solution corresponding to no growth of a nematic wetting layer: so-called partial nematic wetting. Our numerical method of solution depends sensitively on having a sensible trial order parameter profile. There may, of course, be other solutions to the Euler–Lagrange equations of the theory, although we have found what seem to us to be the sensible physical solutions.

The predicted transition from a homeotropic to a distorted profile has been confirmed. The order of the transition seems to be universally first order, although on symmetry grounds a second-order transition seemed possible. We estimate that the first-order transition that we have studied lies typically within O(10^{-4} K) of the bulk nematic–isotropic temperature, making it extremely difficult to identify experimentally.

One possible circumstance in which such a transition might occur is at a free interface. In this case, the signature of the transition would not so much be a jump in layer thickness very close to the bulk transition, as an observed discontinuity in the surface tension at the phase transition which consists of two parts: one the true discontinuity and the other the rapid increase between t_{NI} and t_{HD}. It might in practice be impossible to resolve these two features. However, the observed discontinuity would be $\sigma_{NI}(0) = \sigma_{NI} + W_s^{NI}$, and would be *larger* than the true equilibrium nematic–isotropic surface tension, thus apparently violating the Young–Laplace law, and giving an apparent contact angle θ_s with $\cos\theta_s > 1$.

In addition to assessing and quantifying phenomenological arguments predicting the scaling behaviour of layer width and surface tension associated with the director-distorted wetting phase, we have also found that it has an interesting effect on the prewetting diagram of the Sheng model. Three wetting phases feature in the modified diagram, defining a

wetting triple point which consists of a *kink* in the prewetting line, off which extends a line of layer transitions. This latter feature (which is not a prewetting line in the strict sense) does not terminate in the limit of high surface field.

The origin of the kink may be appreciated from the fact that there is a shift in the value of the surface field at which the wetting transition takes place. This shift is governed by the approximate relation $\Delta g^W \approx \sigma_{NI}(0) - \sigma_{NI}(\pi/2)$ and is brought about by the lowering of the tension of the nematic–isotropic interface when the director is allowed to relax to a parallel orientation.

The effects discussed in this paper depend on the existence of competition between the effect of an imposed surface and that of the spontaneous nematic–isotropic surface. We have discussed this antagonism in the case when $\kappa > 0$ and $g > 0$. We expect somewhat more complex effects, however, in the régime where $\kappa < 0$ and $g < 0$, for which promising results already exist [17].

Acknowledgments

During the course of this work E Velasco was supported by the EPSRC (UK) under grant GR/H68352. F N Braun was supported by an EPSRC CASE studentship in collaboration with DRA Malvern. The British Council supported a visit by T J Sluckin to the Universidad Autónoma, Madrid, where this work was completed. We thank P I C Teixeira, D E Sullivan and C J Walden for instructive and useful conversations and communications.

References

[1] Sullivan D E and Telo da Gama M M 1986 *Fluid Interfacial Phenomena* ed C A Croxton (Chichester: Wiley) p 1
[2] Sluckin T J and Poniewierski A 1986 *Fluid Interfacial Phenomena* ed C A Croxton (Chichester: Wiley) p 215
[3] Sheng P 1976 *Phys. Rev. Lett.* **37** 1059
[4] Sullivan D E and Lipowsky R 1988 *Can. J. Chem.* **66** 553
[5] Sluckin T J and Poniewierski A 1990 *Mol. Cryst. Liq. Cryst.* **179** 349
[6] Beaglehole D 1982 *Mol. Cryst. Liq. Cryst.* **89** 319
[7] Crawford G P, Ondris-Crawford R, Žumer S and Doane J W 1993 *Phys. Rev. Lett.* **70** 1838
[8] Sluckin T J and Poniewierski A 1985 *Phys. Rev. Lett.* **55** 2907
[9] Sen A K and Sullivan D E 1987 *Phys. Rev.* A **35** 1391
[10] Teixeira P I C, Sluckin T J and Sullivan D E 1993 *Liq. Cryst.* **14** 1243
[11] Telo da Gama M M 1984 *Mol. Phys.* **52** 585
[12] de Gennes P G 1971 *Mol. Cryst. Liq. Cryst.* **12** 193
[13] Press W H, Flannery B P, Teukolsky S A and Vetterling W T 1986 *Numerical Recipes: The Art of Scientific Computing* (Cambridge: Cambridge University Press)
[14] Cahn J W 1977 *J. Chem. Phys.* **66** 3367
[15] Langevin D and Bouchiat M A 1973 *C. R. Acad. Sci., Paris* B **277** 731
[16] Poggi Y, Filippini J L and Aleonard E 1976 *Phys. Lett.* **57A** 53
[17] Kothekar N, Allender D W and Hornreich R M 1994 *Phys. Rev.* E **49** 2150